Lawrence Berkeley National Laboratory
Recent Work

Title
Nanoimaging of Organic Charge Retention Effects: Implications for Nonvolatile Memory, Neuromorphic Computing, and High Dielectric Breakdown Devices

Permalink
https://escholarship.org/uc/item/7w33n95p

Journal
ACS Applied Nano Materials, 2(8)

ISSN
2574-0970

Authors
Zhang, Y
Kang, J
Pluchery, O
et al.

Publication Date
2019-08-23

DOI
10.1021/acsanm.9b01182

Peer reviewed

Nano-Imaging and Molecular Insights of Organic Charge Memory Effects

Yingjie Zhang[1,2]*, Jun Kang[3], Olivier Pluchery[4]*, Louis Caillard[4,5], Yves J. Chabal[5], Lin-Wang Wang[3], Javier Fernandez Sanz[7], Miquel Salmeron[3,6]*

[1] Department of Materials Science and Engineering, University of Illinois, Urbana, Illinois 61801, USA.

[2] Frederick Seitz Materials Research Laboratory, University of Illinois, Urbana, Illinois 61801, USA.

[3] Materials Sciences Division, Lawrence Berkeley National Laboratory, Berkeley, CA 94720, USA.

[4] Sorbonne Université, UPMC Univ Paris 06, CNRS-UMR 7588, Institut des NanoSciences de Paris, F-75005, Paris, France

[5] Laboratory for Surface and Nanostructure Modification, Department of Materials Science and Engineering, University of Texas at Dallas, 800 West Campbell Road, Dallas, Texas 75080, USA

[6] Department of Materials Science and Engineering, University of California, Berkeley, CA 94720, USA.

[7] Department Physical Chemistry, Universidad de Sevilla, 41012 Seville (SPAIN)

*Correspondence to: yjz@illinois.edu (Y.Z.), olivier.pluchery@insp.jussieu.fr (O.P.), mbsalmeron@lbl.gov (M.S.)

Abstract

A large variety of organic and molecular materials have been found to exhibit charge memory effects. However, the mechanism of charge storage is not well understood, which is a key bottleneck for the development of stable and scalable organic memory devices. Here study the charge retention mechanism of organic molecules using a model system, a grafted organic monolayer (GOM) on a silicon substrate. Au nanoparticles (NPs) are used as non-destructive nano-electrodes with controlled contact area. Using a scanning probe, we manipulate and image the charge state of the system with nanoscale resolution. We show, via control experiments, that amine functional groups in the GOM molecules play a vital role in charge retention. Density functional simulations show a possible route of molecular distortion that leads to metastable charge states. Our findings shed light to the mechanism of polaronic effects and their role in facilitating charge storage in nanoscale organic systems.

Introduction

Organic and molecular materials have been widely explored for large area electronics applications, such as wearable electronics, solar cells, and display devices (*1–4*). A key difference of such organic systems from inorganic structures is the structural flexibility. On one hand, this has been utilized to fabricate flexible and wearable devices, where the electronic functionalities are not affected by mechanical bending and stretching (*1, 2*). On the other hand, in certain organic materials, the structural reconfiguration is strongly coupled to the electronic states, which can offer new electronic functionality (*5–7*). Remarkably, such strong coupling, or polaronic effect, can occur in the size scale as small as a single layer of molecules. Previously, it has been shown that the conformation, charge, or spin states of certain organic monolayers or single molecules can have two or multiple stable configurations that can be switched in the presence of external stimuli such as light or electric current (*6–12*). This effect is appealing for a variety of applications ranging from non-volatile memory, neuromorphic computing, and high dielectric breakdown devices (*13–15*). However, so far the mechanism behind the charge state – conformation coupling is not well understood, which hinders rational materials and device design.

Here we report a combined experimental and computational study of a model molecular memory system. To facilitate charge state imaging and mechanistic understanding of the memory effect, we prepared a GOM on a silicon substrate, and deposited gold nanoparticles on top as non-destructive electrical contacts to the GOM (*16*). We use a scanning probe tip to contact the NPs and inject charges into the GOM, and to image the surface potential of the NP. The measured potential reflects the charge state of the GOM underneath the NP (*17–19*). We observe a series of charge states at room temperature, which remain stable over a long time (at least 10 hours). We did not monitor the charge state of individual NPs for more than 10 hours, due to the significant thermal drift of our AFM over such long time periods. We examine the role of molecular distortion on charge stabilization through control experiments, density functional theory calculations, and electrostatic modeling.

Results

Materials structure

A schematic of the sample and measurement setup is shown in Fig. 1. An insulating monolayer film of organic molecules ($-(CH_2)_6-CO-NH-(CH_2)_2-NH_2$) was grafted directly on oxide-free, n-doped silicon (phosphorus doped, 2×10^{18} cm^{-3}) (*20, 21*). Au nanoparticles were deposited on top of the GOM (Fig. 1A). The thickness of the GOM was determined to be 1.3 nm by ellipsometry. Due to the substantial contact potential difference (CPD) between Au and the n-doped Si, electrons accumulate in the Au NPs (via tunneling through the GOM) in equilibrium conditions, accompanied by a positive charge depletion layer in the Si. As we showed previously (*17*), the charge state of the NP depends on its radius and can be measured from the change in CPD in the Au NP. This CPD was detected by Kelvin probe force microscopy (KPFM), a non-contact scanning probe microscopy technique.

Charge state manipulation

Before manipulating the charge state of the system, we measured the CPD of the Au NPs using KPFM (Fig. 1A). Then we electrically grounded the tip and applied a bias to the sample (V_s). The tip was then approached towards the NP at a speed of 1–2 nm/s, allowed to contact the NP for a few seconds with a load < 20 nN, and retracted at the same speed (Fig. 1B). After the tip and NP separated, we grounded the sample and acquired KPFM images again (Fig. 1A) to determine any change in the charge state. We performed additional measurements by increasing the compression force during tip-NP contact, and found that similar results were obtained with the sample topography remaining intact for loads up to ~50 nN. This ensures that the change in charge state is not induced by mechanical forces between the tip and the sample.

A typical series of KPFM imaging and manipulation results are shown in Fig. 2. The topographic image in Fig. 2A, obtained simultaneously with the CPD image in Fig. 2B, shows two Au NPs separated by ~100 nm. Charge state manipulation was performed on the 7 nm high NP on the right in the figure, while the untouched NP on the left served as a control. Throughout the whole imaging and manipulation process the topography of the two NPs (height and separation) remained unchanged. We find that while the CPD of the right NP was modified following the process described in Fig. 1, the CPD of the left particle remained constant throughout the whole charging and discharging process. After a tip-NP contact with -1 V sample bias, the CPD of the right NP increased by ~50 mV (from -180 mV to -130 mV) (Fig. 2B,C). This modified charge state remained stable until we contacted the NP again using the tip with V_s=0 V (while the tip was grounded). After this zero bias contact, we found that the CPD of the NP was reset to the original

value (-180 mV) (Fig. 2D), indicating that the charge state of the system was restored. After another tip-NP contact with V_s=1 V, the CPD of the NP decreased by ~80 mV (reaching -260 mV) (Fig. 2E). After a voltage pulse of V_s=-1 V, the system was reset to its original charge state (Fig. 2F). Note that we found a voltage of V_s=0 V did not modify the CPD. The difference in the required discharge voltage for the positive vs negative charged systems are likely due to the asymmetry in the energy landscape of the metastable molecular configurations (NH_2 and NH_3 states), as discussed later.

Following the same procedure, we performed charging and discharging experiments on a series of Au NPs within the size range of 7–9 nm. We were able to alter the charge state of the NP in both directions, up or down, with voltages in the +3 to -3 V range. Fig. 3A summarizes the results on the CPD change after tip contact at different bias. In agreement with the results shown in Fig. 2, positive bias always results in a decrease of CPD, while negative bias leads to an increase of CPD. The other prominent feature in Fig. 3A is that the CPD change is overall larger after the application of a larger bias, revealing the presence of a series of stable charge states. An important observation is that the CPD of the charged Au NP / GOM system remained stable for at least 10 hours in an inert nitrogen atmosphere (in an environmental chamber of the AFM) at room temperature (Supplementary Fig. S1).

We further measured NPs of other sizes, and found similar charging and discharging behavior for all the NPs with diameter between 2.5 nm – 20 nm. Supplementary Fig. S2 shows the charge manipulation results of a 2.5 nm NP.

According to our previous results and calculations (*17*), without tip contact, only one stable charge state exists in electrostatic equilibrium for a given NP size. Therefore, the existence of multiple stable states induced by tip contact could be due to either defects or redox charging in the Si substrate or structural reorganization of the GOM. Although the Si surface could have trace amounts of defects, no surface defect-induced charge memory has ever been reported in Si during the past few decades of research. We thus conclude that the GOM is responsible for the observed memory effect.

Previous work has shown that some molecules with nitro and/or amino groups exhibit conductance switching behaviors (*6–9*), and propose that conformational changes in the molecules could be responsible for such effects. However, to our knowledge there is no published experimental evidence or theoretical calculation to confirm the coupling of molecular conformation to the electrical conductance. To examine whether the amine groups in our GOM are responsible for the observed charge memory effects, we performed the same charging procedures on control samples where the GOM is replaced by a non-aminated molecule -$(CH_2)_6$-COO- (inset of Fig. 3B). We found that no CPD change occurred in the Au NP / non-aminated GOM except at high positive bias ($\geq$ 2 V) (Fig. 3B). However, the CPD change at this high bias is small and irreversible, indicating that it is likely due to permanent damage to the molecules. Therefore, we conclude that the amine group in the GOM is indeed an essential factor contributing to the charge state memory effects in the Au NP-GOM-Si system. As we explain in the following section, the existence of multiple charge states of an Au NP can be explained by the bistable molecular configurations of the series of aminated molecules in contact with the NP.

Density functional theory calculations

To understand how the charge memory effects observed with the aminated GOM molecules could be related to configuration changes of the molecules, we performed Density Functional Theory

(DFT) calculations to determine the energy of the Au NP – aminated molecule system as it adopts different conformations. In the simulation, the (-(CH$_2$)$_6$-CO-NH-(CH$_2$)$_2$-NH$_2$) molecule is initially connected to Au through the amino (NH$_2$) group (Fig. 4A). The Si substrate on the other side of the GOM is not included. After structural relaxation we found two possible distortions leading to final configurations that result in charge retention. We describe here the one that appears more stable. For completeness another is described in the SI. In both models the reference structure has the alkyl chain straight, with its terminal NH$_2$ in the chain end (-CO-NH-(CH$_2$)$_2$-NH$_2$) binding to Au through the N atom (Figs. 4). This binding is the well-known dative bond where the amine group donates its lone pair to form a coordinate covalent Au-N bond (*22*). The description agrees with a Bader analysis (*23*) that shows a net charge transfer (0.17 e$^-$) from the molecule to coordinately unsaturated surface Au atoms. There is another *local* minimum energy configuration, shown schematically in Fig. 4B, where the molecule terminates with an NH$_3$, the H coming from the second CH$_2$ group, and forming a H-bond with the O in the carboxyl group. This configuration bears a positive excess charge, with the Bader analysis indicating a charge transfer to Au of 0.75 e$^-$.

One can go from the NH$_2$ to the NH$_3$ terminated configurations by distortions of the -CO-NH-(CH$_2$)$_2$-NH$_2$ group involving rotations around N-C and C-C bonds which bring the NH$_2$ group close to the C=O group. The energy of several intermediate configurations is shown in Fig. 5A, with schematics of these configurations (labeled a to e) shown in Fig. 5C. We found that all the configurations away from the initial NH$_2$ have higher energy, including the local energy minimum of the final NH$_3$ configuration, which is 0.97 eV higher than that of the initial NH$_2$ ground state. The energy of the configurations from the initial NH$_2$ to the final NH$_3$ goes through a maximum, which exhibits a barrier of 2.2 eV higher that the NH$_2$ configuration (1.23 eV higher than the NH$_3$ configuration).

In the presence of an electric field, either due to the initial charge transfer in the molecular junction, or by the application of an electric bias, the energy landscape of the molecular conformation is altered. We found that an electric field of 2.7 V/nm (positive value denotes downward direction) is able to pull the energy of the NH$_3$ configuration to a level lower than that of the NH$_2$ configuration (Fig. 5B). In this case the activation energy for the transition from NH$_2$ to NH$_3$ configurations is lowered to 1.67 eV. We further calculated the energy difference between the two minimum energy states in the presence of different electric field intensity, with the results shown in Fig. 6A. We observe a critical field value of ~2.5 V/nm, where the energies of the NH$_2$ and NH$_3$ configurations become equal. The higher stability of the NH$_3$ configuration at larger electric fields can be understood by the shift of the Au Fermi level to a position lower than the HOMO level of the -CO-NH-(CH$_2$)$_2$-NH$_2$ group (Fig. S3), which leads to electron transfer from the molecule to the Au. We further found that the wave function of this HOMO level has substantial amplitude around the C-H bonds of the second CH$_2$ group (Fig. S4). Therefore, the loss of an electron from the p$_z$ orbital of the CH$_2$ group (by transfer to Au) can lead to the conversion of CH$_2$ to CH (namely sp^3 to sp^2) and the transfer of the H$^+$ to the terminal NH$_2$ to become NH$_3^+$.

In addition to modifying the energy levels of the molecular configurations, the electric field across the molecular junction also leads to electron tunneling (*17, 21*). These tunneling electrons can excite molecular vibrations (which may involve C-C, C-H, C-N, etc.) that further facilitate the molecular transition from the NH$_2$ to NH$_3$ state (*24–27*). Note that the bending and stretching modes of the molecular bonds have energies below 0.5 eV, which can be easily excited by the tunneling electrons.

Mechanism of multi-stable charge states in molecular arrays

Given that most of the Au NPs have a diameter around 8 nm, we estimate that there are approximately 30 molecules in contact with each NP. Although the configuration with NH_2 termination discussed above is the most stable except at high positive fields (Fig. 6A), we expect that there will always be a non-negligible number of NH_3 terminated molecules under the NP. The local electric field modifies the energy landscape of the molecular conformations (Fig. 5 and Fig. 6A), while the tunneling current further excites molecular vibrations that catalyze the transformation between the NH_2 and NH_3 states. As a result, the portion of molecules in different configurations will change (Fig. 6B and 6C). This induces a modification of the charge state of the Au NP, which depends on the ensemble of molecules and their charge configuration. When the bias is switched off, there is a large (> 1 eV) barrier between the NH_2 and NH_3 configurations of each molecule, which in the absence of tunnel current, prevents charge state switching at room temperature.

To quantify the effect of molecular switching on the potential change of the NP, we performed electrostatic simulations by treating each molecule as a point charge. As shown in Fig. S5, when a molecule switches its charge state from 0 to 1, the change of potential a few nm above the NP surface will be 5 – 10 mV. We can thus estimate that charge state switching of ~30 molecules underneath one NP will induce a few 100s of mV change in the CPD of the NP. Switching of a fraction of these ~30 molecules will lead to smaller CPD changes of the NP. This is consistent with our experimental results shown in Fig. 3A.

Conclusion

In summary, we experimentally observed multi-stable charge memory effects in a molecular model system. We attribute such multi-stable charge states to the bi-stable configurations of individual molecules in the monolayer, and provide a DFT model for a possible atomic-level process that leads to such bi-stability. Our combined experimental and computational results provide mechanistic insights into the polaron-induced molecular memory effects.

Materials and Methods

Sample preparation. Au nanoparticle synthesis and organic monolayer preparation was described before [Caillard 2013, Caillard 2015] (*17, 20*). The substrate is Si(111) doped with phosphorus (carrier concentration: 2×10^{18} cm^{-3}). Before performing KPFM measurements, the sample was annealed in nitrogen glovebox at 140 °C for 30 min.

Kelvin probe force microscopy measurements. KPFM was performed using a home-built setup operated in the single-pass, frequency modulation mode (*17–19*). The tip is Ti/Pt coated Si, with a spring constant of ~ 2 N/m and a resonance frequency of ~ 70 kHz. Measurements were done in a sealed chamber continuously purged with nitrogen. The measured CPD was calibrated by setting the CPD of the GOM to zero in each image. During the measurements the sample remain oxide-free as evident from the uniform CPD distribution on the GOM surface (*17*).

References and Notes

1. H. Lee, E. Kim, Y. Lee, H. Kim, J. Lee, M. Kim, H.-J. Yoo, S. Yoo, Toward all-day wearable health monitoring: An ultralow-power, reflective organic pulse oximetry sensing patch. *Sci. Adv.* **4**, eaas9530 (2018).

2. J. Y. Oh, S. Rondeau-Gagné, Y.-C. Chiu, A. Chortos, F. Lissel, G.-J. N. Wang, B. C. Schroeder, T. Kurosawa, J. Lopez, T. Katsumata, J. Xu, C. Zhu, X. Gu, W.-G. Bae, Y. Kim, L. Jin, J. W. Chung, J. B.-H. Tok, Z. Bao, *Nature* **539**, 411–415 (2016).

3. J. You, L. Dou, K. Yoshimura, T. Kato, K. Ohya, T. Moriarty, K. Emery, C.-C. Chen, J. Gao, G. Li, Y. Yang, A polymer tandem solar cell with 10.6% power conversion efficiency. *Nat. Commun.* **4**, 1446 (2013).

4. E. H. Kim, S. H. Cho, J. H. Lee, B. Jeong, R. H. Kim, S. Yu, T.-W. Lee, W. Shim, C. Park, Organic light emitting board for dynamic interactive display. *Nat. Commun.* **8**, 14964 (2017).

5. J. Ren, N. Vukmirovic, L.-W. Wang, Nonadiabatic molecular dynamics simulation for carrier transport in a pentathiophene butyric acid monolayer. *Phys. Rev. B* **87**, 205117 (2013).

6. N. Xin, J. Wang, C. Jia, Z. Liu, X. Zhang, C. Yu, M. Li, S. Wang, Y. Gong, H. Sun, G. Zhang, Z. Liu, G. Zhang, J. Liao, D. Zhang, X. Guo, Stereoelectronic effect-induced conductance switching in aromatic chain single-molecule junctions. *Nano Lett.* **17**, 856–861 (2017).

7. A. S. Blum, J. G. Kushmerick, D. P. Long, C. H. Patterson, J. C. Yang, J. C. Henderson, Y. Yao, J. M. Tour, R. Shashidhar, B. R. Ratna, Molecularly inherent voltage-controlled conductance switching. *Nat. Mater.* **4**, 167–172 (2005).

8. J. Chen, M. A. Reed, A. M. Rawlett, J. M. Tour, Large on-off ratios and negative differential resistance in a molecular electronic device. *Science* **286**, 1550–1552 (1999).

9. E. Lörtscher, J. W. Ciszek, J. M. Tour, H. Riel, Reversible and controllable switching of a single-molecule junction. *Small* **2**, 973–977 (2006).

10. F. Schwarz, G. Kastlunger, F. Lissel, C. Egler-Lucas, S. N. Semenov, K. Venkatesan, H. Berke, R. Stadler, E. Loertscher, Field-induced conductance switching by charge-state alternation in organometallic single-molecule junctions. *Nat. Nanotech.* **11**, 170–176 (2016).

11. J. L. Zhang, J. Q. Zhong, J. D. Lin, W. P. Hu, K. Wu, G. Q. Xu, A. T. S. Wee, W. Chen, Towards single molecule switches. *Chem. Soc. Rev.* **44**, 2998–3022 (2015).

12. H. Bi, C.-A. Palma, Y. Gong, P. Hasch, M. Elbing, M. Mayor, J. Reichert, J. V. Barth, Voltage-driven conformational switching with distinct raman signature in a single-molecule junction. *J. Am. Chem. Soc.* **140**, 4835–4840 (2018).

13. C. Simão, M. Mas-Torrent, N. Crivillers, V. Lloveras, J. M. Artés, P. Gorostiza, J. Veciana, C. Rovira, A robust molecular platform for non-volatile memory devices with optical and magnetic responses. *Nat. Chem.* **3**, 359–364 (2011).

14. Y. van de Burgt, E. Lubberman, E. J. Fuller, S. T. Keene, G. C. Faria, S. Agarwal, M. J. Marinella, A. A. Talin, A. Salleo, A non-volatile organic electrochemical device as a low-voltage artificial synapse for neuromorphic computing. *Nat. Mater.* **16**, 414–418 (2017).

15. K. Yang , X. Huang, J. He, P. Jiang, Strawberry-like core–shell Ag@Polydopamine@BaTiO$_3$

hybrid nanoparticles for high- k polymer nanocomposites with high energy density and low dielectric loss. *Adv. Mater. Interfaces* **2**, 1500361 (2015).

16. G. Puebla-Hellmann, K. Venkatesan, M. Mayor, E. Lörtscher, Metallic nanoparticle contacts for high-yield, ambient-stable molecular-monolayer devices. *Nature* **559**, 232–235 (2018).

17. Y. Zhang, O. Pluchery, L. Caillard, A. F. Lamic-Humblot, S. Casale, Y. J. Chabal, and M. Salmeron, Sensing the charge state of single gold nanoparticles via work function measurements. *Nano Lett.* **15**, 51–55 (2015).

18. Y Zhang, D Ziegler, M Salmeron, Charge trapping states at the SiO2-oligothiophene monolayer interface in field effect transistors studied by Kelvin probe force microscopy. *ACS Nano* **7**, 8258–8265 (2013).

19. Y. Zhang, D. Zherebetskyy, N. D. Bronstein, S. Barja, L. Lichtenstein, D. Schuppisser, L.-W. Wang, A. P. Alivisatos, M. Salmeron, Charge percolation pathways guided by defects in quantum dot solids. *Nano Lett.* **15**, 3249–3253 (2015).

20. D. Aureau, Y. Varin, K. Roodenko, O. Seitz, O. Pluchery, and Y. J. Chabal, Controlled deposition of gold nanoparticles on well-defined organic monolayer grafted on silicon. *J. Phys. Chem. C* **114**, 14180–14186 (2010).

21. O. Pluchery, Y. Zhang, R. Benbalagh, L. Caillard, J. J. Gallet, F. Bournel, A.-F. Lamic-Humblot, M. Salmeron, Y. J. Chabal, F. Rochet, Static and dynamic electronic characterization of organic monolayers grafted on a silicon surface. *Phys. Chem. Chem. Phys.* **18**, 3675–3684 (2016).

22. Venkataraman, H. J. Choi, S. G. Louie, M. S. Hybertsen, J. B. Neaton, Amine-gold linked single-molecule circuits: experiment and theory. *Nano Lett.* **7**, 3477–3482 (2007).G.

23. G. Henkelman, A. Arnaldsson, H. Jónsson, A fast and robust algorithm for Bader decomposition of charge density. *Comput. Mater. Sci.* **36**, 354–360 (2006).S. Y. Quek, L.

24. B. C. Stipe, M. A. Rezaei, W. Ho, Coupling of vibrational excitation to the rotational motion of a single adsorbed molecule. *Phys. Rev. Lett.* **81**, 1263 (1998).

25. S. Maier, I. Stass, X. Feng, A. Sisto, A. Zayak, J. B. Neaton, M. Salmeron, Dehydrogenation of ammonia on Ru(0001) by electronic excitations. *J. Phys. Chem. C* **119**, 10520–10525 (2015).

26. A. Mugarza, T. K. Shimizu, D. F. Ogletree, M. Salmeron, Chemical reactions of water molecules on Ru(0001) induced by selective excitation of vibrational modes. *Surf. Sci.* **603**, 2030–2036 (2009).

27. T. K. Shimizu, A. Mugarza, J. I. Cerdá, M. Heyde, Y. Qi, U. D. Schwarz, D. F. Ogletree, M. Salmeron, Surface species formed by the adsorption and dissociation of water molecules on a Ru(0001) surface containing a small coverage of carbon atoms studied by scanning tunneling microscopy. *J. Phys. Chem. C* **112**, 7445–7454 (2008).
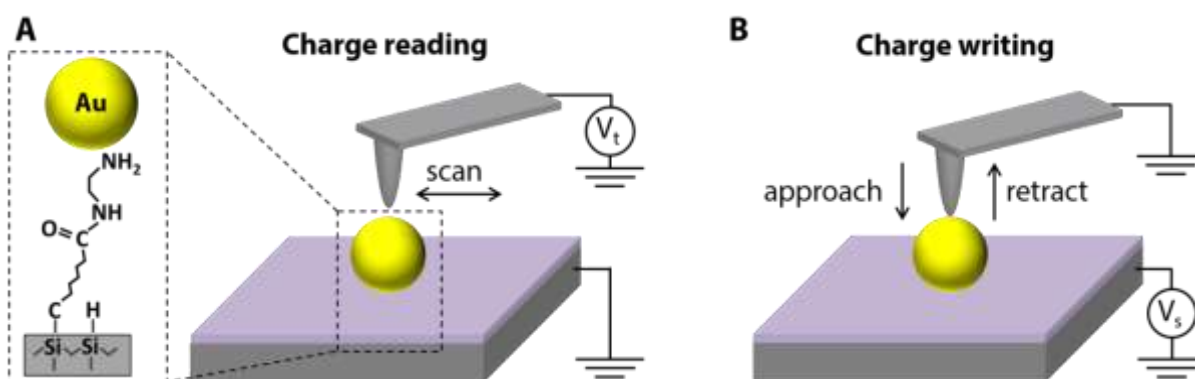
Figure 1. Schematic of the device and measurement setup. (**A**) Left: molecular structure of the hybrid tunnel junction consisting of silicon / grafted organic monolayer (GOM) / Au nanoparticle (NP). Right: Charge state imaging by Kelvin probe force microscopy (KPFM). (**B**) Charge state manipulation by applying an electric bias (to the sample) while the tip is in contact with the Au NP. V_t: tip bias. V_s: sample bias.
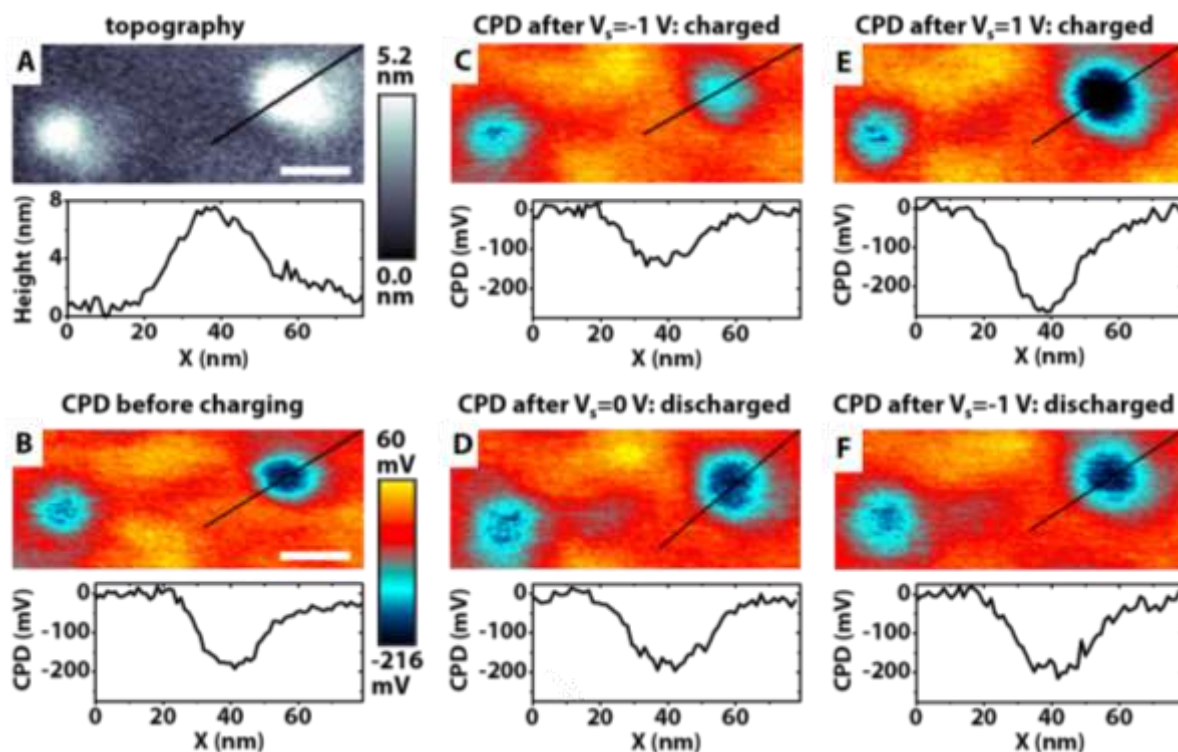

Figure 2. Charge state manipulation of the am-hybrid system. (**A**) Topographic image of two NPs. The one on the right (with a height of ~7 nm) was approached by the tip to manipulate the charge state, while the one on the left was not contacted during the whole process. (**B**) Original CPD image of the two NPs on GOM/Si substrate before tip contact. (**C**) After tip-NP contact with -1 V sample bias, the tip was lifted to image the CPD of the NPs with the substrate grounded. (**D**–**F**) Similar with (C), CPD of the NPs were imaged after tip-sample contact with different sample bias applied, as labeled. Scale bar: 30 nm. All the images were taken at the same area and have the same size scale. The CPD color scale in (C–F) is the same as that in (B).
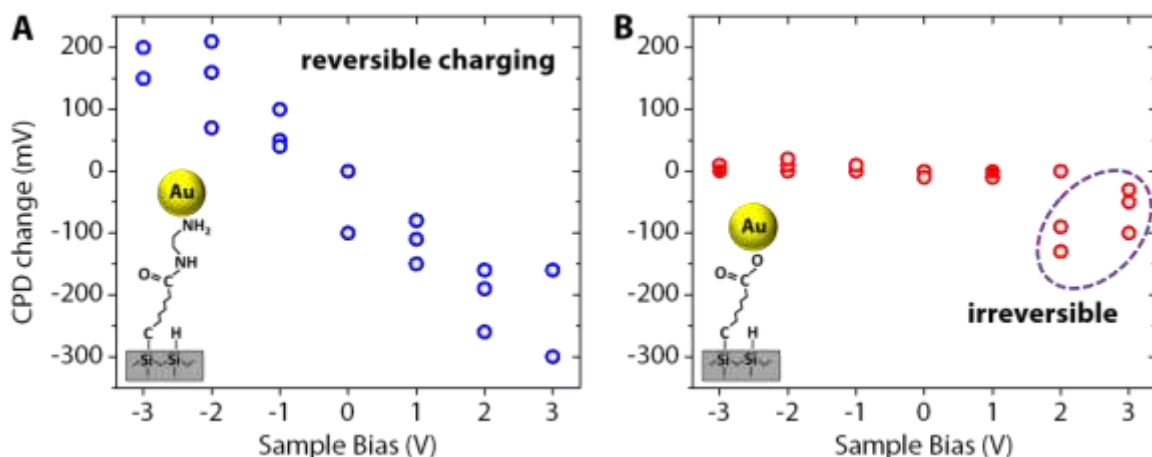
Figure 3. Charge writing at different bias and with different molecules. (**A**) Si/GOM/Au NP tunnel junction with aminated molecules exhibits bias-tunable (the sample bias applied during tip-NP contact), reversible charging effects. (**B**) The junction with non-aminated molecules exhibits no charging effects in the bias range of -3 V – 1 V, while small, irreversible CPD changes were observed with 2 V – 3 V bias. Each hollow circle represents one data point, while each solid circle represents two overlapping data points.
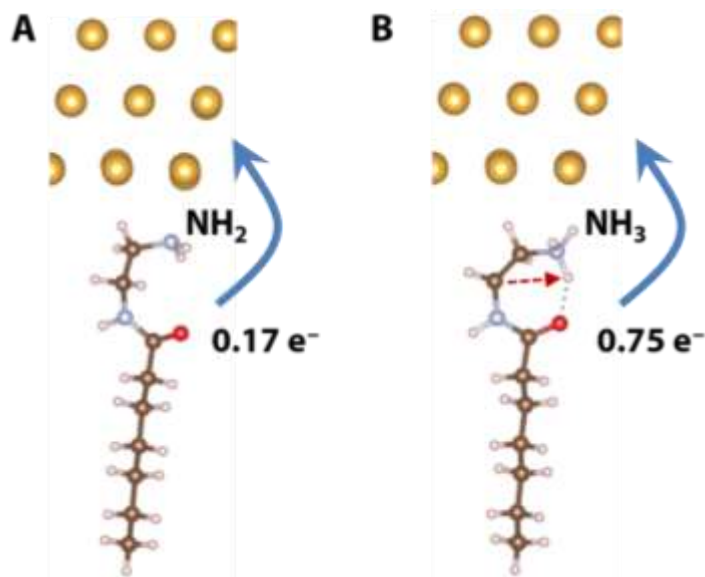

Figure 4. Bi-stability of the molecular configuration. (**A**) A stable, minimum energy configuration where the terminal NH_2 group hybridizes with Au; the resulting amount of Bader charge transfer is 0.17 e⁻. (**B**) A possible meta-stable configuration as a result of proton transfer. A distortion of the molecular end group leads to a proton transfer from a CH_2 group to the terminating NH_2 group, resulting in the formation of NH_3. In this case the Bader charge transfer to Au is 0.75 e⁻. This configuration is another minimum energy state relative to small distortions.
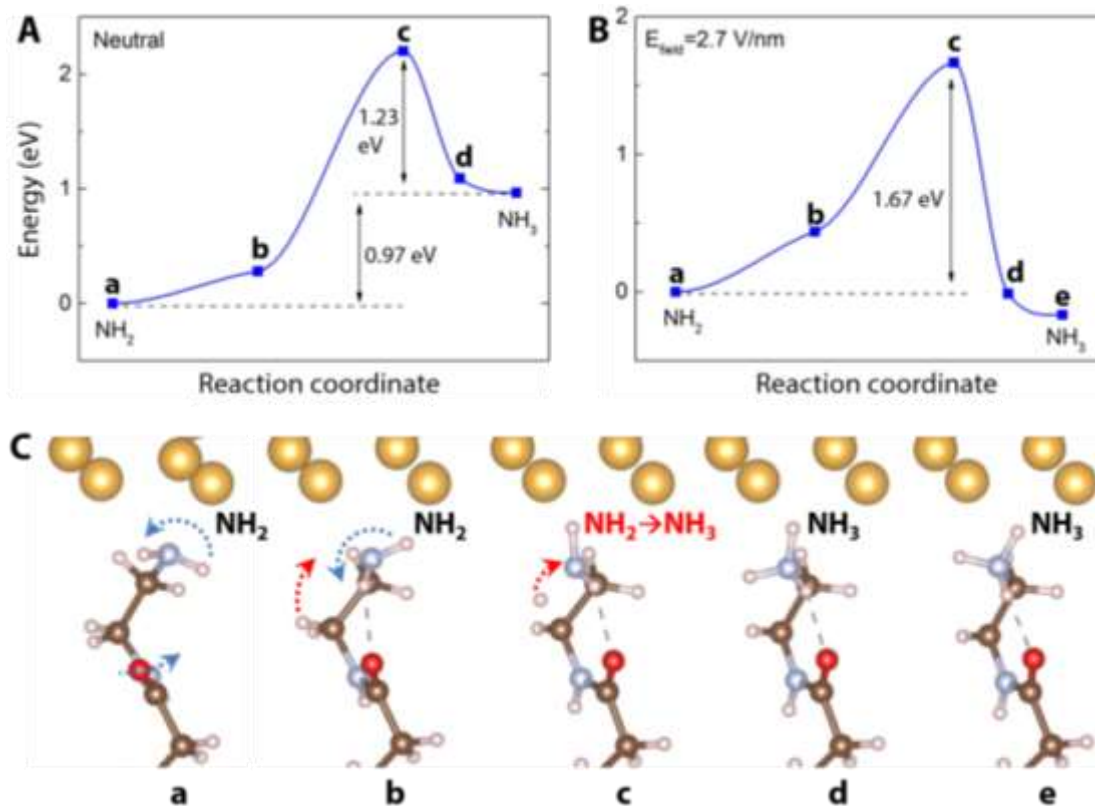
Figure 5. Energy landscape of various molecular configurations. (**A**) A series of possible molecular configurations in the absence of an external electric field. An energy barrier separates two minimum energy configurations, and the NH_2 termination is the most stable state. (**B**) Energy landscape in the presence of a positive 2.7 V/nm electric field (pointing downwards). In this case the NH_3 termination is the most stable. (**C**) Schematic structures of the intermediate configurations (from **a** to **e**) corresponding to the states labeled in (A) and (B).
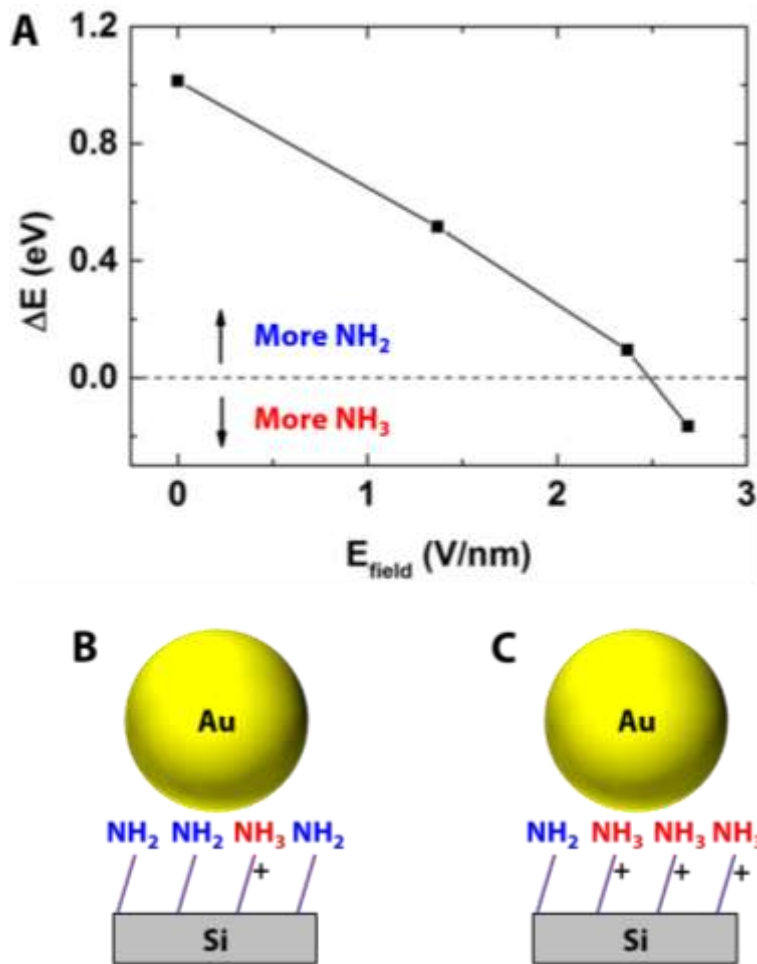
Figure 6. Multi-charge stability of the Au NP – organic monolayer system. (**A**) Energy difference between the NH_2 and NH_3 terminated configurations as a function of applied electric field (pointing downwards). (**B**) A schematic showing that there are more NH_2 groups (neutral) than NH_3 groups (positively charged) underneath the Au NP, in the presence of a zero or small electric field (<2.5 V/nm). (**C**) A schematic showing more NH_3 groups than NH_2 groups, in the presence of a large electric field (>2.5 V/nm).

Supporting Information

Nano-Imaging and Molecular Insights of Organic Charge Memory Effects

Yingjie Zhang[1,2]*, Jun Kang[3], Olivier Pluchery[4]*, Louis Caillard[4,5], Yves J. Chabal[5], Lin-Wang Wang[3], Javier Fernandez Sanz[7], Miquel Salmeron[3,6]*

[1] Department of Materials Science and Engineering, University of Illinois, Urbana, Illinois 61801, USA.
[2] Frederick Seitz Materials Research Laboratory, University of Illinois, Urbana, Illinois 61801, USA.
[3] Materials Sciences Division, Lawrence Berkeley National Laboratory, Berkeley, CA 94720, USA.
[4] Sorbonne Université, UPMC Univ Paris 06, CNRS-UMR 7588, Institut des NanoSciences de Paris, F-75005, Paris, France
[5] Laboratory for Surface and Nanostructure Modification, Department of Materials Science and Engineering, University of Texas at Dallas, 800 West Campbell Road, Dallas, Texas 75080, USA
[6] Department of Materials Science and Engineering, University of California, Berkeley, CA 94720, USA.
[7] Department of Physical Chemistry, Universidad de Sevilla, 41012 Seville (SPAIN)

*Correspondence to: yjz@illinois.edu (Y.Z.), olivier.pluchery@insp.jussieu.fr (O.P.), mbsalmeron@lbl.gov (M.S.)
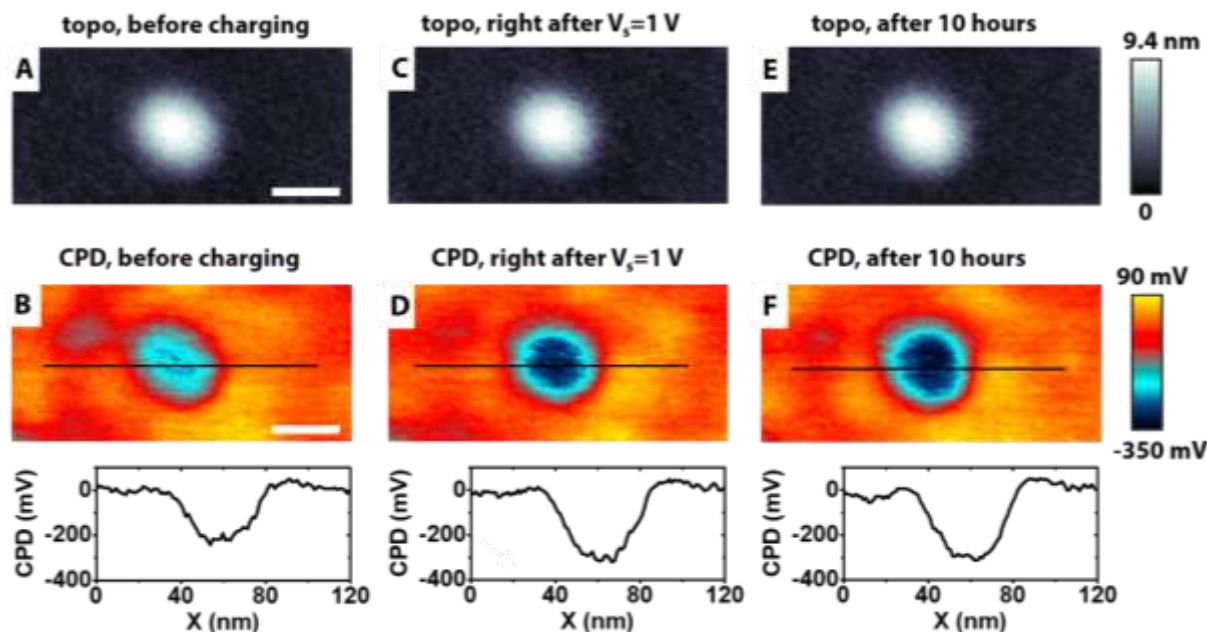
Charge retention test

Figure S1. Charge retention test of the am-hybrid system. (**A**) and (**B**) are the topographic and CPD images of a NP, showing a height of ~8 nm and a CPD of -220 mV. After tip-NP contact with 1 V sample bias, the tip was lifted to image the CPD of the NP with the substrate grounded. The topographic and CPD images, shown in (**C**) and (**D**), reveal that the height remained constant (~8 nm) while the CPD decreased to -300 mV. After 10 hours, the height (**E**) and CPD (**F**) remained unchanged (~8 nm, -300 mV), confirming that the charge stored in the NP is stable for at least 10 hours.

Charge manipulation of NPs with different sizes

In addition to Au NPs with a size range of 7–9 nm, which is the focus of Fig. 2 and Fig. 3 in the main text, we measured other NPs with sizes varying between 2.5 nm – 20 nm. These NPs all showed similar charge memory effects. Results on the 2.5 nm NP are shown in Figure S2. We also performed control measurements where the AFM (atomic force microscopy) tip was positioned on the GOM surface (instead of the NP) followed by the same charge writing and

imaging procedures (*1*). In this case no charging effect was observed, indicating that the presence of Au NP is essential for charge memory effects.
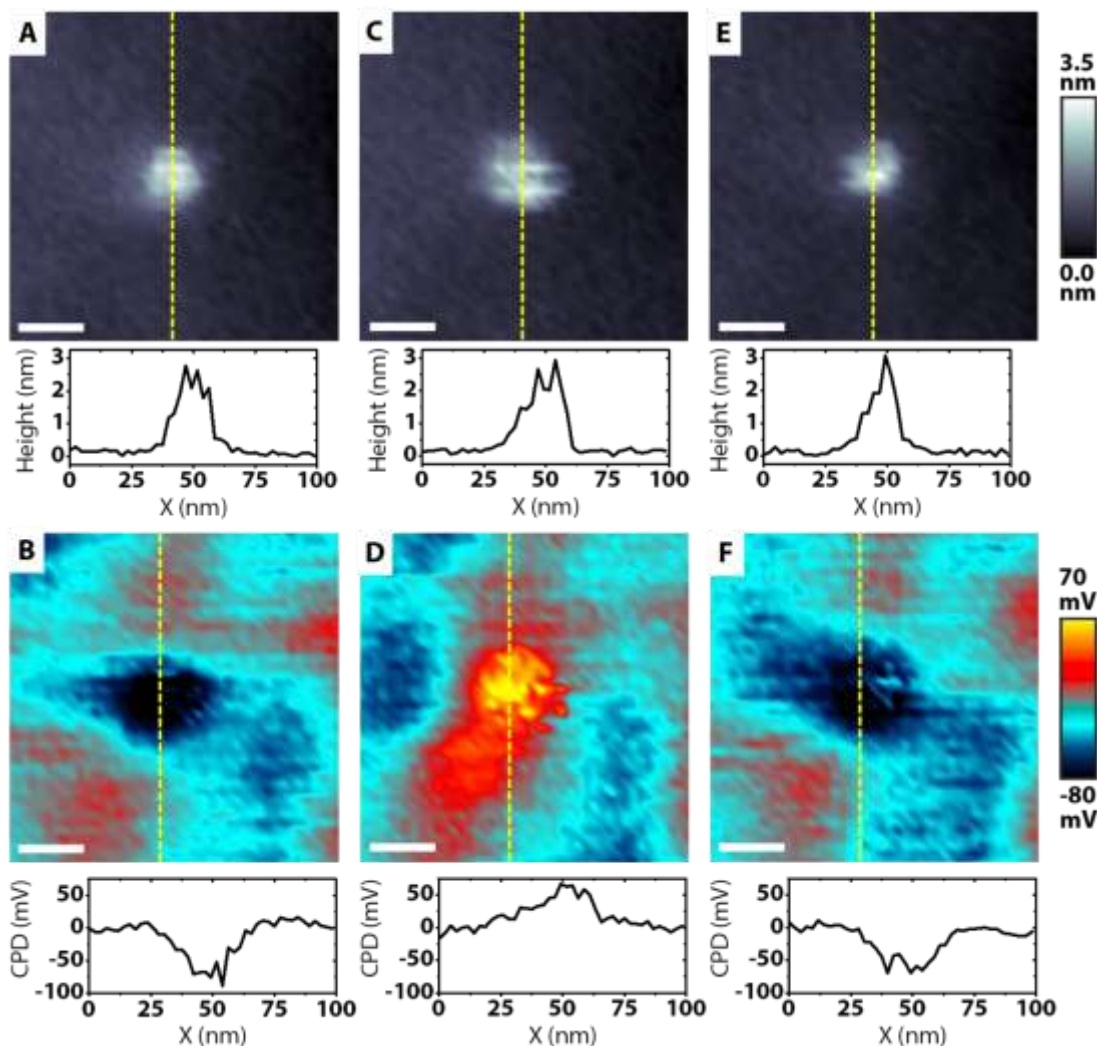

Figure S2. Charge state manipulation of an am-hybrid system with 2.5 nm Au NP. (**A** and **B**) Original topography and CPD image of a NP on top of the organic monolayer. Height and CPD of the NP are 2.5 nm and about -70 mV, respectively. A charging protocol was performed with -3 V sample bias applied during tip-NP contact. After this process, the height of the NP remained unchanged (**C**), while the CPD increased to approximately 60 mV (**D**). After discharging (tip-NP contact with 0 V sample bias), the height of the NP still remained constant (**E**) and CPD decreased to about -60 mV (**F**), close to the original CPD value. Scale bars: 20 nm. The color scales in (A, C, E) and in (B, D, F) are the same, as labeled on the right of (E) and (F).

DFT calculations

Models and computation details
All calculations are carried out using the Vienna ab initio simulation package (VASP) (*2*). The core−valence interaction is described by the projector-augmented wave (PAW) method (*3*). The wavefunctions are expanded in a plane-wave basis set with a 500 eV cutoff. Structure relaxation is stopped when the force on each atom is smaller than 0.01 eV/Å. The generalized gradient approximation of Perdew−Burke−Ernzerhof (GGA-PBE) (*4*) is adopted for the exchange-correlation functional. The Brillouin zone was sampled using a (3x3x1) gamma-centered mesh of k-points in the slab calculations, and the gamma-point in NP model. To obtain faster convergence, thermal smearing of one-electron states ($k_BT = 0.05$ eV) was allowed using the Gaussian smearing method to define the partial

occupancies. Energy barriers were calculated by the climbing-image nudged elastic band method (*5*). Gold NPs surfaces were represented by a slab built up from a (4x4) supercell, 4 atomic layers thick. A vacuum of 25 Å was allowed between the slabs.

DOS of the NH$_2$ and NH$_3$ configurations under different electric field

In Fig. S3, the DOS of the aminated molecule + Au systems with the NH$_2$ and NH$_3$ configurations (see Fig. 4 for the structure) and under different electric field are shown. At zero field, the NH$_2$ configuration is more stable, and its HOMO level is fully occupied. Under a 2.7 V/nm field, the HOMO level of the NH$_2$ configuration is partially occupied, and it is less stable than that of the NH$_3$ configuration. In contrast, the HOMO of the NH$_3$ configuration is always partially occupied, indicating a significant charge transfer from the molecule to Au. This is more clearly seen in Fig. S4, where the charge density within the energy window [E$_{Fermi}$, E$_{Fermi}$+0.25 eV] for the NH$_3$ configuration at zero field is given. The empty p$_z$ state near the second C group can be identified, which stabilizes the NH$_3$ configuration.
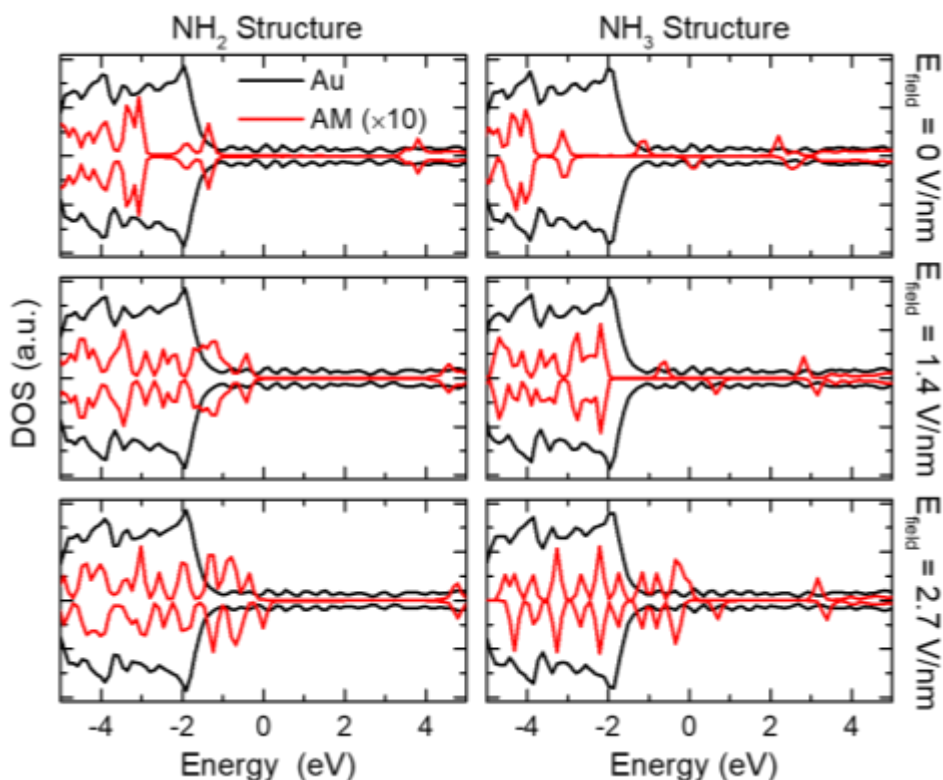

Figure S3. The DOS of the aminated molecule (AM) + Au systems with the NH$_2$ and NH$_3$ configurations and under different electric field. To make the figure clear, the DOS of the molecule is multiplied by a factor of 10.
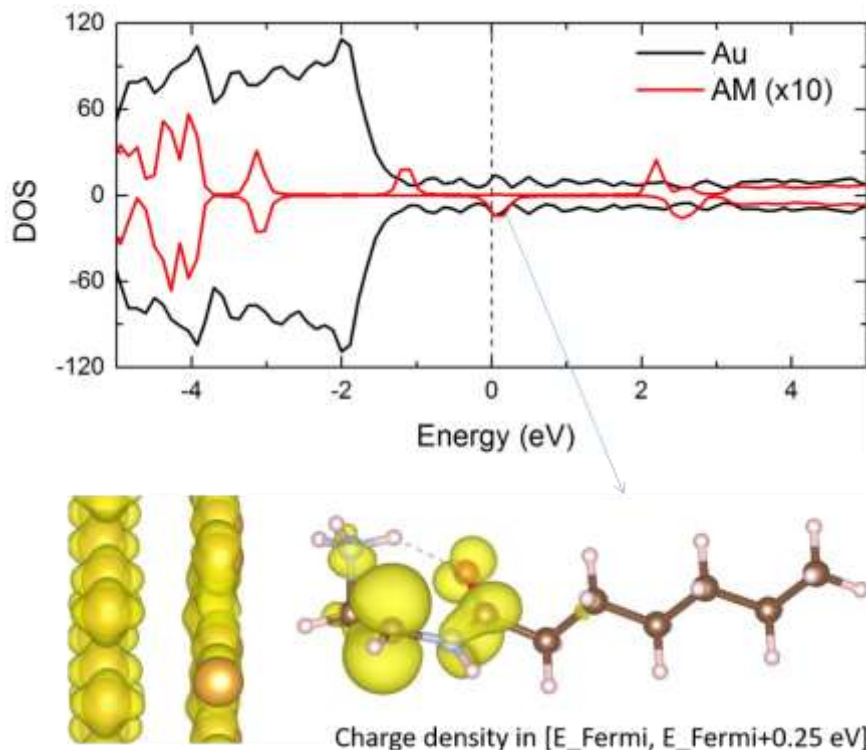
Figure S4. DOS of the aminated molecule (AM) +Au systems in the NH_3 configuration showing the orbitals involved in the transfer of charge to Au. The charge density within the energy window [E_{Fermi}, E_{Fermi}+0.25 eV] is shown, in which the empty p_z state near the second C group can be clearly seen. To make the figure clear, the DOS of the molecule is multiplied by a factor of 10.

Alternative polaronic distortion model

As mentioned in the main text, we explored also different conformation models. Here we present one that does not involve transfer of H from the CH_2 group to the terminal NH_2. Two molecular conformations are calculated: a linear one (L), as in the model in the main text, and a chelated model (C), formed by a rotation around the C-N bond that brings the oxygen atom in the CO group to the surface. This results in the formation of a bidentate bond to the surface involving the N and the O atoms. These are shown in Figure S5. DFT calculations including Van der Waals corrections *(6,7)* show that mode C is a bit more stable than mode L by 0.21 eV, so that at RT both modes should coexist. A Bader analysis shows that the amount of electron charge transferred to the Au NP in this arrangement is larger: -0.23 e$^-$.

Figure S5. Linear (left) and chelated (right) models. The transition state between these states involves a rotation around the C-N bond, as indicated.
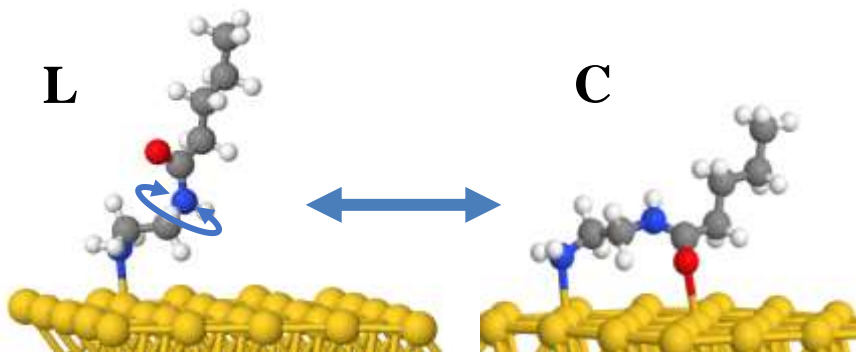
When an electric field is included in the simulations the C configuration is stabilized; for example with a field of -0.25 V/ Å, C is 0.38 eV more stable than L. Also, the stronger the field the larger the stabilization, with 0.44 eV for -0.3 V/ Å. Once the field is switched off the system will evolve to its equilibrium C/L ratio. Yet, to accomplish this

passage involves surpassing a barrier where the O-Au bond breaks, which we have estimated to be 0.43 eV using a Au_{54} nanocluster as model for the metal.

When a positive field of +0.3 V/ Å was applied no significant changes were observed in the energy of the L configuration, except that now it is the organic molecule which appears slightly negatively charged by -0.11e. However, the C configuration becomes unstable, with detachment of the CO group from the surface and evolving to the linear configuration.

While both this and the main text model can explain charge transfer and a bi-stable system of two configurations. However, given that the alkyl end of the molecule is covalently attached to the Si substrate and thus immobile, the alternative model presented here may require additional molecular rearrangements to accommodate the larger space needed to accommodate the additional site on the Au surface required for the formation of the chelating CO-Au bond.

Electrostatic simulations

We can simplify the AM as a point charge, and the Au NP as a conducting sphere with a fixed potential determined by the sample bias (Fig. S5). This sphere of radius R is localized at the origin (0, 0, 0). It has a fixed potential V_0. A point charge q is placed at $(0, 0, -d)$. Then the potential φ at a point (x, y, z) outside the sphere is:

$$\varphi(x, y, z) = \frac{1}{4\pi\varepsilon_0} \left[\frac{q}{\sqrt{x^2 + y^2 + (z+d)^2}} - \frac{qR/d}{\sqrt{x^2 + y^2 + (z+R^2/d)^2}} + \frac{V_0 R}{\sqrt{x^2 + y^2 + z^2}} \right]$$

When the charge on AM changes Δq, using the simple model, the potential change $\Delta\varphi$ is:

$$\Delta\varphi(x, y, z) = \frac{1}{4\pi\varepsilon_0} \left[\frac{\Delta q}{\sqrt{x^2 + y^2 + (z+d)^2}} - \frac{\Delta q R/d}{\sqrt{x^2 + y^2 + (z+R^2/d)^2}} \right]$$

In the experiment, $R\sim3.5$ nm. The DFT optimized d is $R+0.41$ nm (0.41 nm is the distance between the net charge center of AM and the Au surface). Considering $\Delta q=+1$ e, the potential change on the x=0 plane is shown in Fig. S6. When $\Delta q > 0$ (corresponding to NH_2-NH_3 transformation), $\Delta\varphi$ on the tip side ($z>0$ region) is always positive. This trend is consistent with the experimental observation that when the sample bias decreases, the CPD increases.
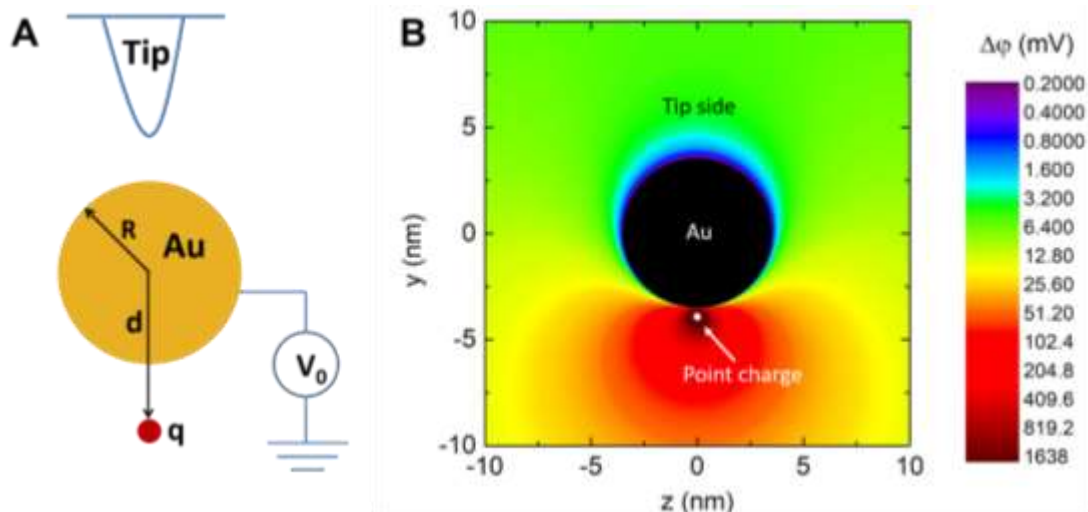

Figure S6. (**A**) Simplified point charge and conducting sphere model. (**B**) The potential change $\Delta\varphi$ when $\Delta q=+1$ e, with $R=3.5$ nm and $d=3.91$ nm. The white dot indicates the position of the point charge, and the black region indicates the conducting sphere.

References

28. O. Pluchery, Y. Zhang, R. Benbalagh, L. Caillard, J. J. Gallet, F. Bournel, A.-F. Lamic-Humblot, M. Salmeron, Y. J. Chabal, F. Rochet, Static and dynamic electronic characterization of organic monolayers grafted on a silicon surface. *Phys. Chem. Chem. Phys.* **18**, 3675–3684 (2016).
29. G. Kresse, J. Furthmüller, Efficient iterative schemes for ab initio total-energy calculations using a plane-wave basis set. *Phys. Rev. B* **54**, 11169–11186 (1996).

30. G. Kresse, D. Joubert, From ultrasoft pseudopotentials to the projector augmented-wave method. *Phys. Rev. B* **59**, 1758–1775 (1999).
31. J. P. Perdew, K. Burke, M. Ernzerhof, Generalized gradient approximation made simple. *Phys. Rev. Lett.* **77**, 3865–3868 (1996).
32. G. Henkelman, B. P. Uberuaga, H. Jonsson, A climbing image nudged elastic band method for finding saddle points and minimum energy paths. *J. Chem. Phys.* 113, 9901–9904 (2000).
33. J. Klimeš, D.R. Bowler, A. Michaelides. *Phys. Rev. B.* 2011, 83, 195131.
34. J. Klimeš, D.R. Bowler, A. Michaelides. *J. Phys.: Cond. Matt*. 2010, 22, 022201.